ADVANCED FUNCTIONAL MATERIALS
www.afm-journal.de

Multifunctional Upconversion Nanoparticles for Dual-Modal Imaging-Guided Stem Cell Therapy under Remote Magnetic Control

*Liang Cheng, Chao Wang, Xinxing Ma, Qinglong Wang, Yao Cheng, Han Wang, Yonggang Li, and Zhuang Liu**

Stem cells have generated a great deal of excitement in cell-based therapies. Here, a unique class of multifunctional nanoparticles (MFNPs) with both upconversion luminescence (UCL) and superparamagnetic properties is used for stem cell research. It is discovered that after being labeled with MFNPs, mouse mesenchymal stem cells (mMSCs) are able to maintain their viability and differentiation ability. In vivo UCL imaging of MFNP-labeled mMSCs transplanted into animals is carried out, achieving ultrahigh tracking sensitivity with a detection limit as low as ≈10 cells in a mouse. Using both UCL optical and magnetic resonance (MR) imaging approaches, MFNP-labeled mMSCs are tracked after being intraperitoneally injected into wound-bearing mice under a magnetic field. The translocation of mMSCs from the injection site to the wound nearby the magnet is observed and, intriguingly, a remarkably improved tissue repair effect is observed as the result of magnetically induced accumulation of stem cells in the wound site. The results demonstrate the use MFNPs as novel multifunctional probes for labeling, in vivo tracking, and manipulation of stem cells, which is promising for imaging guided cell therapies and tissue engineering.

1. Introduction

Mesenchymal stem cells (MSCs) are multipotent cells that can differentiate into a variety of mesenchymal tissues, and have shown great promise as a potential source of cell-based therapies, such as amyotrophic lateral sclerosis, acute myocardial infarction, liver cirrhosis, Parkinson's disease, and repairing of various damaged tissues.[1–6] However, the in vivo noninvasive monitoring of stem cells after transplantation with high sensitivity and accuracy in the host body is one critical issue remains to be resolved in this field. Labeling MSCs with reporter genes and the use of corresponding optical imaging techniques provide a noninvasive method for tracking and quantifying the fate of administered MSCs in vivo.[7,8] This approach, although is a powerful tool in animal studies, has limited value in terms of clinical translation.[7,9,10] On the other hand, several different methods to label stem cells with exogenous probes including quantum dots (QDs),[11,12] magnetic nanopartciles,[13–15] carbon nanotubes,[16] and silicon nanoparticles[17] have also been developed for in vivo stem cell tracking via various imaging modalities such as optical imaging, magnetic resonance imaging (MRI), and radionucleotide based imaging.[15,18,19] However, due to the intrinsic limits of current imaging techniques and tracking probes, the accurate detection of small numbers of cells, as well as the remote control of stem cells translocation after in vivo transplantation, remains challenging in stem cell research.

In recent years, near-infrared (NIR) excited upconversion nanoparticles (UCNPs), usually based on lanthanide-containing nanocrystals, have attracted intensive interest due to their great potentials in various fields including biomedicine.[20–26] In comparison with classical down-conversion fluorescent probes (such as QDs and dyes), UCNPs show large anti-Stokes shift, sharp emission bands, high resistance to photobleaching, and importantly, minimal autofluorescence background signals that allow sensitive imaging and detection in biological systems. In addition, a large number of reports have evidenced that UCNPs show low toxicity in vitro to cells and in vivo to animals.[27–29] Owing the above-mentioned advantages of UCNPs, many groups including us have explored UCNPs as novel optical nanoprobes in biomedical imaging and detection.[24,30–35] Owing to the absence of autofluorescence background, the

Dr. L. Cheng, C. Wang, Y. Cheng, Prof. Z. Liu
Jiangsu Key Laboratory for Carbon-Based Functional Materials & Devices
Institute of Functional Nano & Soft Materials Laboratory (FUNSOM)
Soochow University
Suzhou, Jiangsu 215123, China
E-mail: zliu@suda.edu.cn
X. X. Ma, Dr. Y. G. Li
Department of Radiology
the First Affiliated Hospital of Soochow University
Suzhou, Jiangsu 215123, China
Q. L. Wang, H. Wang
Laboratory of Developmental Genetics and Genomics Medical College
Soochow University
Suzhou 215123, China

DOI: 10.1002/adfm.201201733

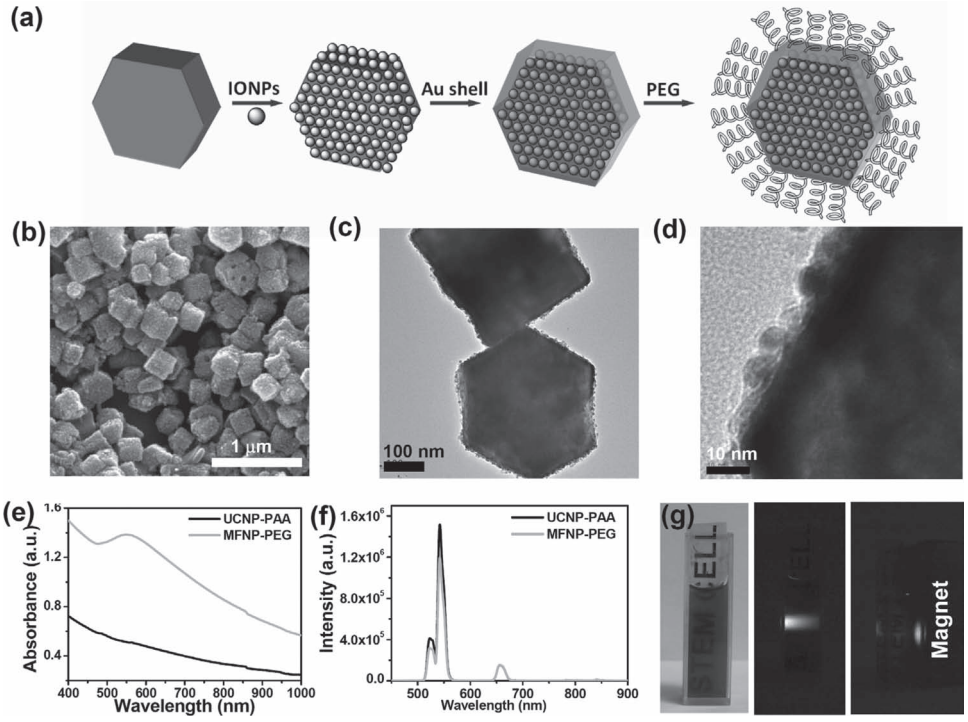

Figure 1. Multifunctional upconversion nanoparticles used for stem cell tracking. a) A schematic illustration showing the composition of MFNP-PEG. b) SEM image of MFNPs. c) TEM image of MFNPs. d) A high-resolution TEM image on the surface of a MFNP. e) UV-vis-NIR absorption spectra of UCNP-PAA and MFNP-PEG solutions. f) UCL spectra of UCNP-PAA and MFNP-PEG solutions at the same Y^{3+} concentration. g) Photographs of a MFNP-PEG sample in the aqueous solution under ambient light (left), exposed to a 980 nm laser (middle), and with a magnet (right).

UCNP-based upconversion luminescence (UCL) imaging appears to be much more sensitive than QD-based in vivo fluorescence imaging.[36] In vivo multimodal imaging based on UCNPs has also been demonstrated recently.[31,37] With UCNPs as labeling probes, ultrasensitive detection of cells in small animals has further been realized in a number of latest studies.[38,39]

Recently, we developed a layer-by-layer (LBL) assembly approach to synthesize a class of MFNPs consisting of a UCNP particle as the core, a layer of ultrasmall iron oxide nanoparticles (IONPs) as the intermediate shell, and a thin layer of gold as the outer shell (**Figure 1**a).[31] Those MFNPs after functionalized with polyethylene glycol were used for upconversion luminescence (UCL)/magnetic resonance multimodal imaging as well as magnetically targeted photothermal ablation of cancer in vitro and in vivo.[31,32] Herein, we use PEG conjugated MFNPs to label mMSCs, whose proliferation and differentiation potentials are found to be not obviously affected after MFNPs labeling, for ultrasensitive in vivo whole-body stem cell tracking by both UCL optical and MR imaging techniques. Owing to the strong magnetism of our MFNPs, we successfully show that the in vivo translocation of mMSCs labeled with nanoparticles after being injected into mice can be remotely controlled by applying a local magnetic field. Highly efficient magnetically targeted accumulation of MNFP-labeled mMSCs is observed in the wound site nearby a magnet, where remarkably enhanced tissue repairing is realized afterwards. Our work demonstrates imaging-guided externally-controlled stem cell translocation and therapy in vivo, and promises future explorations of multifunctional nanoprobes in stem cell research.

2. Results and Discussion

2.1. Functionalization and Characterization of MFNPs

Polyethylene glycol (PEG)-functionalized MFNPs were synthesized as described in our previous report (Figure 1a).[31] Firstly, Yb and Er doped $NaYF_4$ UCNPs (Y:Yb:Er = 69:30:1) with the diameter of ≈180 nm were synthesized following a literature procedure and modified with poly (acrylic acid) (PAA, MW = 1800) via a ligand exchange method at high temperature. Magnetic nanoparticles (Fe_3O_4) with an average diameter of 5 nm were modified with dopamine (DA) and then attached on the surface of UCNPs through the electrostatic force. Afterwards, a thin layer of Au shell (2–3 nm) was grown on the surface of UCNP-IONP nanocomposite by seed-mediated growth, obtaining composite MFNPs with an average diameter of ≈220 nm and the molar ration of Y:Fe:Au to be 100:37:4 as determined by inductively coupled plasma atomic emission spectroscopy (ICP-AES) (Figure 1b–d).[31] The Au shell could not only be used to facilitate surface PEG coating on nanoparticles by the thiol-gold chemistry, but also offer NIR absorbance useful for photothermal therapy and photoacoustic imaging.[16,32] The as-prepared MFNPs were then functionalized by lipoic acid conjugated PEG to improve their water solubility and biocompatibility. The hydrodynamic diameter of PEGylated MFNPs (MFNP-PEG) was ≈240 nm (Supporting Information Figure S1), a little larger than the TEM result. MFNP-PEG solution was deep purple in color and well dispersed in various physiological solutions including saline, cell medium, and

serum (Figure 1g, Supporting Information Figure S2). UV-vis-NIR absorption spectrum of MFNP-PEG showed a broad resonance absorption band from 400 nm to 1000 nm (Figure 1e), which was consistent with the plasmon resonance frequencies observed in similar Au nanostructures.[40] After the growth of the IONP layer and gold shell, ≈88% UCL emission of MFNPs at 540 nm was retained compared to PAA modified UCNPs (Figure 1f). As shown and discussed in our previous report, the layer of IONPs could prevent the direct contact between the UCNP surface and the Au shell, and significantly reduce the luminescence quenching of the Au nanostructure to UCNPs.[31] The lack of obvious hysteresis loops in field-dependent magnetization measurement indicated the superparamagnetic nature of the IONPs and those composite MFNPs (Supporting Information Figure S3).[31] T2-weight MR images of MFNPs acquired on a 3.0-T MR scanner revealed the concentration-dependent darkening effect, with the transverse relaxivity (R_2) of MFNPs measured to be 320.1 $mM^{-1}S^{-1}$ (Supporting Information Figure S3). Due to their strong magnetism, MFNPs could be rapidly attacked by a magnet placed nearby (Figure 1g).

2.2. Stem Cell Labeling with MFNP-PEG

We next used MFNPs for stem cell labeling. mMSCs were obtained from the bone marrow of healthy Balb/C mice by the standard protocol and characterized by their specific surface antigen expressions using flow cytometry (Supporting Information Figure S4).[41,42] For cell labeling, mMSCs were incubated with MFNP-PEG for 4 h. After washing with PBS to remove free nanoparticles, stem cells labeled with MFNPs were imaged by a modified laser scanning confocal microscope. It was found that mMSCs incubated with MFNPs showed quite strong UCL emission. As expected, the cellular uptake of MFNPs increased as the rise of MFNP-PEG concentrations (**Figure 2**a,c). MR imaging was also used to evaluate the cell uptake efficiency of MFNPs. We observed that the T2-weighted MR signals of mMSCs decreased with the increase of MFNP-PEG concentrations after 4 h incubation (Figure 2b,d). No significant UCL signals were observed from mMSCs incubated with MFNP-PEG under 4 °C (Supporting Information Figure S5), suggesting that the cellular uptake of those nanoparticles could likely via the energy

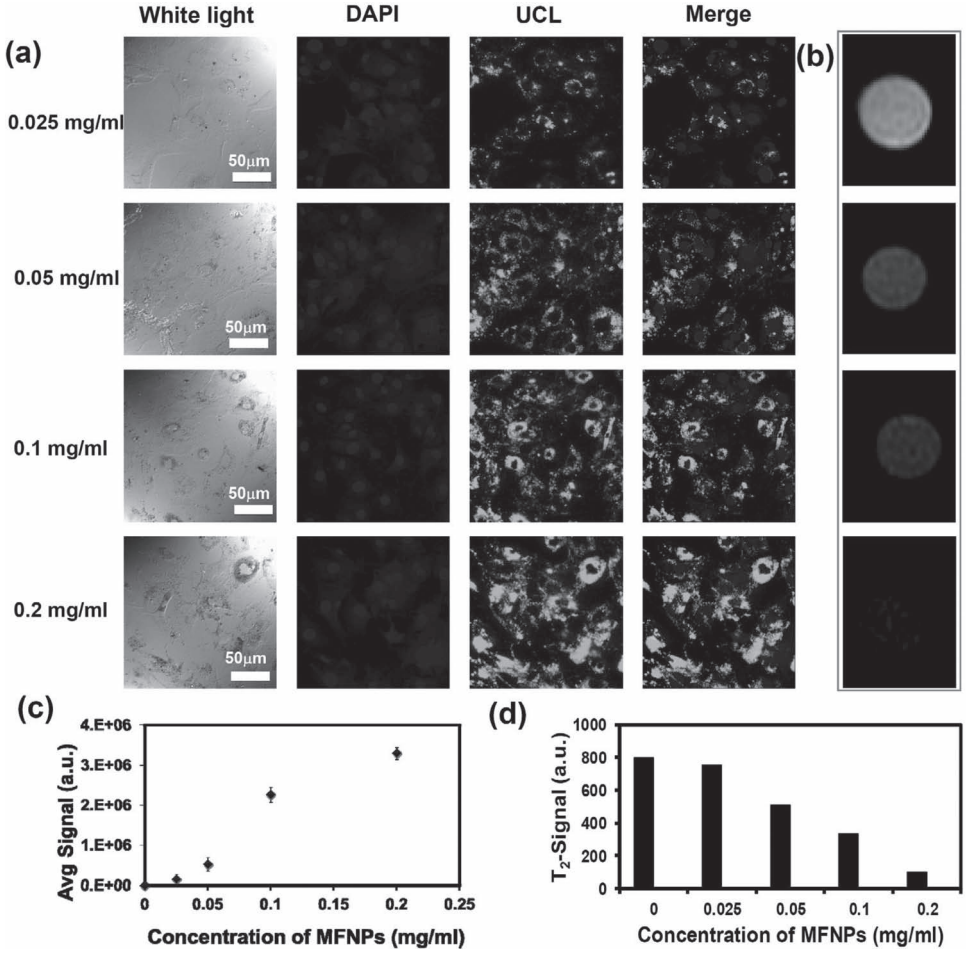

Figure 2. Stem cell labeling with MFNPs. a) Confocal UCL images of mMSCs labeled with MFNP-PEG at different concentrations at 0.025 mg/mL, 0.05 mg/mL, 0.1 mg/mL, and 0.2 mg/mL. All images were taken under the identical instrumental condition and presented at the same intensity scale. b) T2-weighted MR images of mMSCs labeled with different concentrations of MFFNP-PEG. c) Quantified UCL signal intensities in (a). d) Quantified T2-weighted MR signal intensities in (b).

dependent endocytosis mechanism,[43] although further carefully studies are needed to fully illustrate the detailed cell entry pathways and intracellular fates of those relatively big nanoparticles.

The labeling probes could leak out from stem cells over time by exocytosis, a common problem in stem cell tracking which leads to the uptake of these probes by other nearby cells, introducing false positive signals.[44,45] We thus investigated this issue by a transwell culture system. MFNP-labeled mMSCs were cultured in the upper compartment of the transwell culture system, while unlabeled mMSCs were grown in the lower compartment. The upper and lower compartments were separated by a porous membrane that allowed the passing of free nanoparticles but not cells. Although the UCL intensity from MFNP-labeled cells cultured in the upper compartment decreased over time due to the cell proliferation that diluted intracellular nanoparticle concentrations, no obvious signal in unlabeled cells cultured in the lower compartment was observed after 10 days (Supporting Information Figure S6), suggesting that MFNPs could be used in stem cell tracking over a relatively long period without significant leakage from labeled cells.

2.3. Interactions of MFNPs with Stem Cells

Numerous reports have investigated the toxicology of UCNPs in vitro and in vivo. It generally accepted that the toxicity of UCNPs is closely associated to their size and the surface chemistry.[27,29] Before using MFNP-PEG for stem cell tracking, we must understand how MFNPs with large diameters (≈240 nm) interact with mMSCs. A number of methods from various aspects were used to evaluate the potential cellular toxicity of MFNPs to mMSCs. Standard cell viability assay uncovered no decrease in relative viabilities of MFNPs labeled mMSCs at the concentration up to 0.5 mg/mL (Supporting Information Figure S7). Release of lactate dehydrogenase (LDH) is an indicator of cell membrane damage, which leads to cell necrosis. To further look for any potential cell damage caused by MFNPs, LDH release from MFNPs labeled mMSCs was also examined. It was found that the levels of released LDH from MFNPs labeled mMSCs were normal compared to that of untreated mMSCs, indicating no obvious cell membrane damage induced by MFNPs (**Figure 3**a).

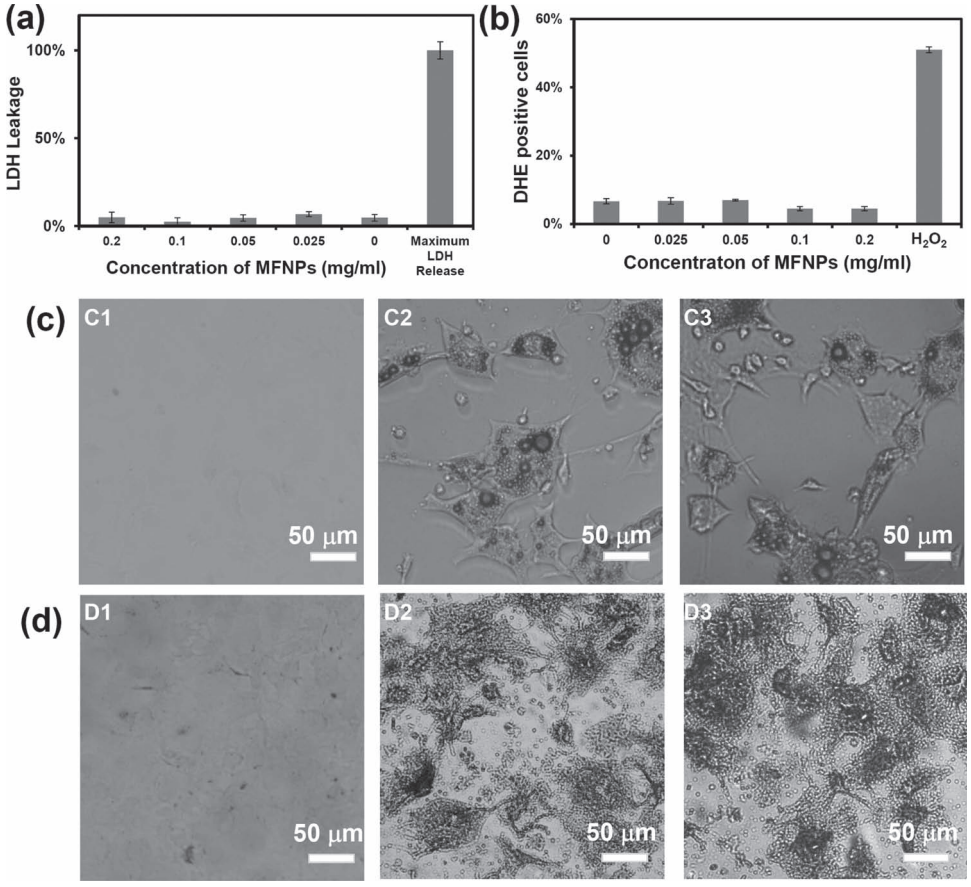

Figure 3. Toxicity of MFNPs to mMSCs. a) Percentage of LDH leakage of mMSCs after various treatments indicated. b) Generation of intracellular ROS determined by DHE staining and FACS measurement after various treatments indicated. Error bars are based on triplicate samples at minimum. c,d) Differentiation of mMSCs labeled with MFNPs. mMSCs labeled with MFNP-PEG (0.1 mg/mL) were differentiated to adipocytes and osteoblasts in vitro and stained with ORO and ARS, respectively. c) ORO stained unlabeled mMSCs(C2) and MFNP-labeled mMSCs (C3) after being cultured in adipogenic culture for 2 weeks. d) ARS stained unlabeled mMSCs (D2) and MFNP-labeled mMSCs (D3) after being cultured in osteogenic culture for 2 weeks. Normally cultures mMSCs without differentiation were also stained by ORO (C1) or ARS (D1)) as negative controls.

Reactive oxygen species (ROS) such as $\bullet O^{2-}$, $\bullet OH$, and H_2O_2 can damage biomacromolecules such as DNA, proteins, and lipids, resulting in a high degree of cytotoxicity. In this study, intracellular peroide and superoxide levels in mMSCs were assessed using a dihydroethidine (DHE) probe. No significant increase in the percentage of DHE positive cells after treatment with different concentrations of MFNPs was noticed, suggesting minimal oxidative stress induced to stem cells after MFNP-labeling (Figure 3b and Supporting Information Figure S8).

mMSCs can differentiate into various cell types including osteoblasts, chondrocytes, myocytes, adipocytes, and others, a unique behavior useful in tissue repairing and regeneration.[46,47] We next investigated the impact of MFNP-labeling to the differentiation capability of mMSCs. Following adipogenic differentiation (Figure 3C1–C3) and osteogenic differentiation (Figure 3D1–D3), Oil-red-O (ORO) and Alizarin-red-S (ARS) staining were carried out to visualize lipid vacuoles and calcium deposits, respectively, revealing that mMSCs labeled with MFNPs had similar differentiate capabilities compared with normal unlabeled mMSCs (Figure 3c,d). Our data collectively suggest that PEGylated MFNPs have no obvious toxicity to mMSCs even at the high concentration, and more significantly, would not impact the differentiation of labeled stem cells.

2.4.In vivo Stem Cell Tracking

To explore the possibility and detection sensitivity of MFNP-labeled stem cells, various numbers of mMSCs labeled with MFNPs were subcutaneously injected onto the back of a nude mouse, which was then imaged by a modified Maestro in vivo imaging system with an external 980 nm laser as the excitation source. Strong UCL signals were detected on sites injected with MFNP-labeled mMSCs (**Figure 4**a). Quantification of UCL emissions showed an increase of integrated UCL intensities as the increase in cell numbers. Remarkably, as few as ≈10 MFNP-labeled mMSCs transplanted into the mouse could be successfully detected, showing a much higher sensitivity than QD-based cell tracking under fluorescence imaging and IONP-based cell tracking under MR imaging, as the detection limits of the latter two techniques are usually no fewer than thousands of cells[18,48] (Figure 4b). The ultra-high sensitivity in MFNP-based in vivo stem cell tracking at almost the single cell level (it is experimentally difficult to implant a single cell into a mouse) is attributed to the absence of background auto-fluorescence of biological tissues in UCL imaging,[36] whereas in traditional down-conversion fluorescence imaging, the strong tissue auto-fluorescence largely limits its detection sensitivity. It is worth noting that for our current MFNPs based visible emitting UCNPs, the tissue depth during imaging is ≈5–7 mm,[49] which, however, could be easily increased to >15 mm if NIR emitting Tm^{3+}/Yb^{3+} co-doped UCNPs are used as demonstrated by Li and co-workers in their recent report.[50]

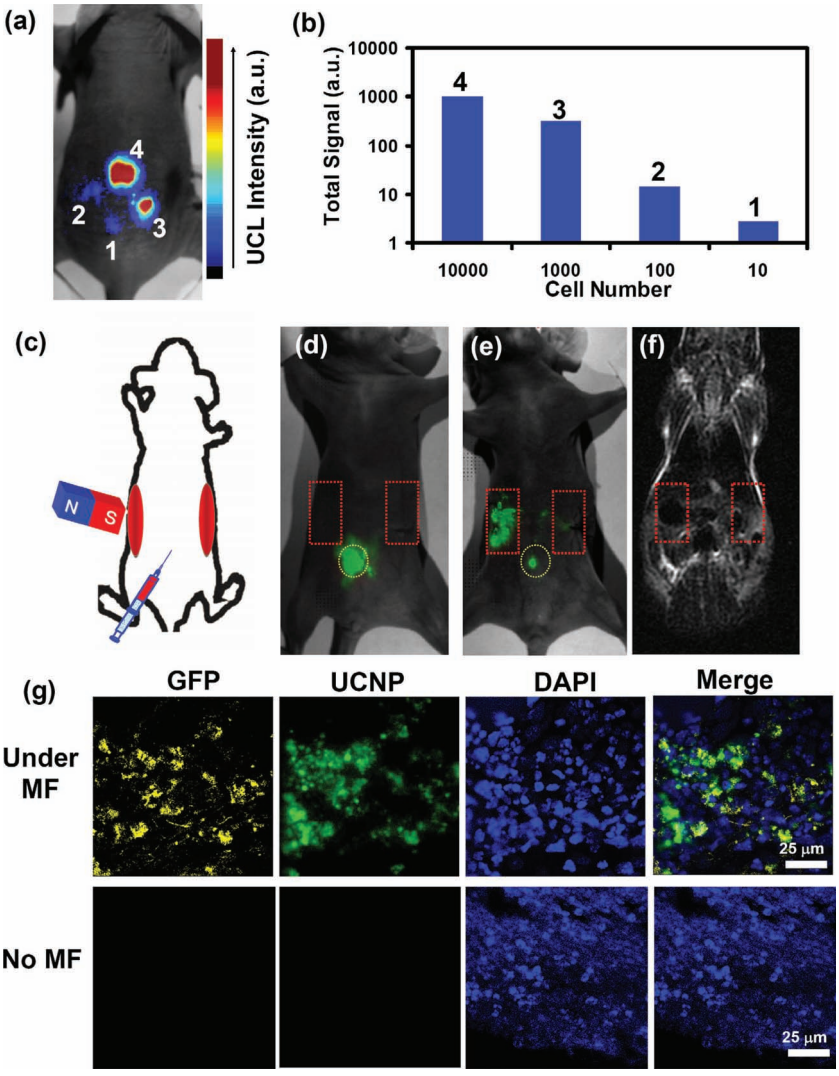

Figure 4. In vivo tracking of MFNP-labeled mMSCs. a) A UCL image of a mouse subcutaneously injected with various numbers of mMSCs (≈10 to 10^4) labeled with MFNP-PEG. b) Quantification of UCL signals in (a). c–f) Magnetic wound targeting. c) A scheme showing the experimental design. The wound-bearing mouse was anaesthetized by isoflurane inhalation and i.p. injected with MFNP-labeled mMSCs. A magnet was attached to the left-side wound for 6 h before imaging. d,e) UCL images of a mouse injected with MFNP-labeled mMSCs taken right after injection (d) and 6 h after injection in the presence of a magnetic field (e). f) In vivo MR image of the same mouse in (e). Two wounds were highlighted by red rectangles while the initial injection site was highlighted by a yellow circle. g) Confocal images of wound slices taken from the magnet side (upper row) and the opposite side (lower row). Cell nuclei were stained by diamidino-phenylindole (DAPI). Yellow, green and blue colors represent GFP, MFNP and DAPI signals, respectively.

2.5. In Vivo Multimodal Imaging of Wound Under Magnetically Targeting

Several earlier reports have demonstrated that the in vivo movement of cells labeled with magnetic nanoparticles could be manipulated by applying a magnetic field.[51–55] Our previous study have shown that MFNPs could be used for UCL/MR multimodal imaging as well as in vivo magnetically targeted cancer treatment.[32] We thus wondered whether the translocation of MFNP-labeled stem cells could be remotely controlled by an external magnetic field. In vitro experiments verified that MFNP-labeled mMSCs in the presence of a magnetic field could rapidly move toward the magnet within a few minutes (Supporting Information Figure S9).

Inspired by the in vitro results, we next investigated magnetically induced stem cell translocation in vivo. To build the wound model, two wounds with diameters of ≈0.8 cm were drawn on two sides of abdomen of each mouse by skin peeling-off. MFNP-labeled mMSCs were then intraperitoneally (i.p.) injected in the middle of the abdomen. Magnetic targeting was conducted by binding a small magnet to the wound on one side of each mouse (Figure 4c). A modified Maestro in vivo fluorescence imaging system was used to detect MFNP-labeled stem cells after transplantation. As expected, extremely bright UCL signals were observed 6 hours later from the wound site with the magnet attached, while the other wound on the opposite side showed neglectable UCL signals (Figure 4d,e, Supporting Information Figure S10), suggesting controlled translocation of MFNP-labeled mMSCs under magnetic targeting. Similar results were also observed by T2-weighted MR imaging, which showed obvious darkening effect in the wound site exposed to the magnetic field (Figure 4f). Quantification of UCL images showed a nearly 30-fold increase of UCL signals in the wound under the magnetic field compared to the un-targeted control. Consistently, T2-weighted MR signals in wound with magnetically targeted stem cell accumulation decreased by ≈80% compared to the wound on the other side without a magnet (Supporting Information Figure S11). Thus in vivo UCL/MR dual-modal imaging revealed the excellent magnetic wound targeting effect of MFNP-labeled mMSCs.

To verify the observed UCL/MR signals in the wound site were indeed from labeled mMSCs rather than free nanoparticles, mMSCs were transfected with green fluorescent protein (GFP) and then labeled with MFNPs before being i.p. injected into a wound-bearing mouse. After 6 hours, the mouse was scarified and the two wounds in the presence or absence of a magnetic field were taken out for ultrathin frozen section (10 μm in thickness). Confocal images of the wound slices (Figure 4g) uncovered that in the wound under magnetic targeting, strong GFP and UCL signals from MFNP-labeled MSCs were observed, in marked contrast to the other side of wound without magnetic targeting. Importantly, the GFP and UCL signals were well co-localized, demonstrating that UCL/MR signals detected in vivo were due to MFNP-labeled MSCs, rather than free nanoparticles (Supporting Information Figure S12).

2.6. Tissue Repairing

In recent years, MSCs have come to be recognized as one type of stem cells actively participating in tissue repairing.[47,56–58] Various studies have indicated that when tissue damage occurs, MSCs are able to migrate into the damaged tissue to facilitate tissue repairing. Although the mechanism of MSC-mediated tissue repairing is complicated, it is believed that MSC-derived growth factors play an important role. Additionally, MSCs must interact closely with various stromal cells and inflammatory cells once they reach the site of damage to participate in tissue repairing. Thus how to enhance the migration of implanted MSCs to the site of damage could be of great interest in stem cell therapies.

Therefore, we next studied the wound repair efficacy in BALB/c mice treated with MFNP-labeled mMSCs. Mice (n = 8) with two wounds on both left and right sides of the abdominal skin were i.p. injected with MFNP-labeled mMSCs. A magnetic field was applied on one wound of each mouse by placing a magnet close to the left side of the mouse abdomen for 6 h (**Figure 5**a). Figure 5b showed the in vivo UCL images of mice at different time points after implantation of MFNP-labeled mMSCs. It was found that the majority of injected mMSCs stayed inside the magnetically targeted wounds within 2 weeks.

Then we investigated the healing up of wounds over time. Careful measurements of wounds at 3, 7, and 14 days post treatment indicated that those wounds exposed to the magnetic field exhibited accelerated wound closure in BALB/c mice, compared to those on the other side of mice without magnetically targeted stem cell accumulation (Figure 5c,d). Histological evaluation of two sides of wounds in BALB/c mice at 2 weeks (Figure 5e,f) post treatment also suggested enhanced re-epithelialization in treated wounds under magnetic targeting compared to the untargeted control. To our best knowledge, this is the first time that imaging-guided enhanced in vivo tissue repairing by using magnetic field induced stem cell wound targeting is realized in animal experiments. Future applications of this strategy involving the use of external control to manipulation the translocation of labeled stem cells under the guidance of multimodal imaging, may offer new opportunities to stem cell based therapies and tissue engineering, and are potentially valuable for many pre-clinical investigations when controlled cell implantation to specific lesions is required, as well as for clinical treatment to achieve improved therapeutic efficacy.

3. Conclusions

In summary, MFNPs based on Au shelled UCNP-IONP nanocomposites with unique optical and magnetic properties are synthesized and used for in vivo multimodal labeling, tracking, and manipulation of stem cells. It is found that MFNP-labeling neither induces noticeable toxicity to mMSCs, nor affects their ability to differentiate. Due to the absence of background autofluorescence of biological tissues in UCL imaging, the in vivo UCL imaging of MFNP-labeled mMSCs transplanted into animals achieves ultra-high tracking sensitivity with as few as ≈10 cells detectable in a mouse. We further track MFNP-labeled mMSCs after i.p. injection in the presence of a magnetic field, and observe magnetically induced translocation of mMSCs to the wound site nearby a magnet. Significantly enhanced tissue repairing is further achieved, owing to the controlled mMSCs accumulation in the wound under magnetic field, as well as the retained activities and functions of stem cells after MFNP-labeling. Our results highlight the promise of using MFNPs as

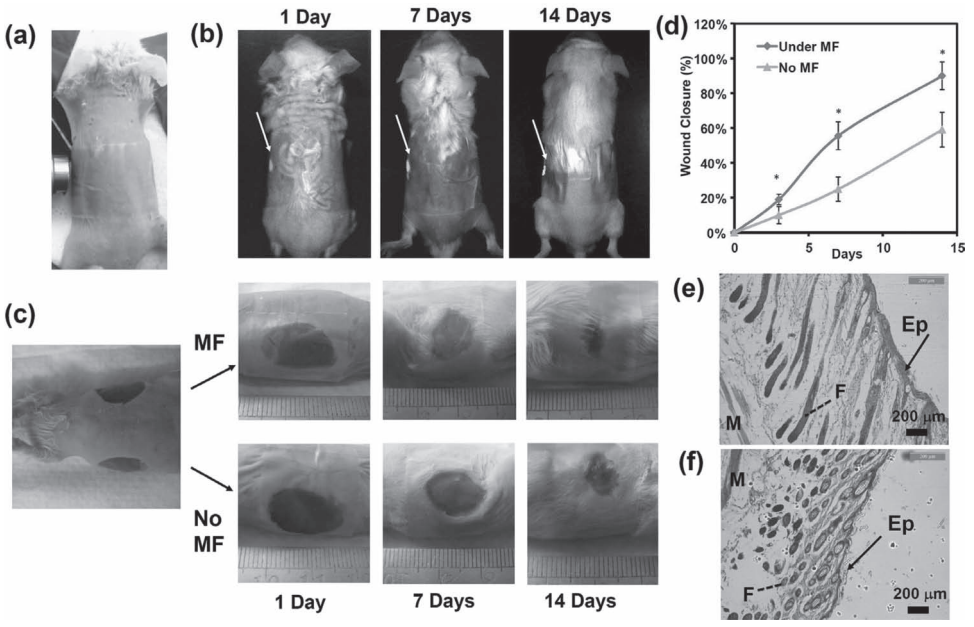

Figure 5. Magnetic field induced tissue repairing. a) A photograph of a mouse with one of its two wounds attached to a magnet. The magnetic field was applied right after injection of mMSCs and removed 6 h later. b) In vivo UCL images of a mouse taken at 1 day, 7 days, and 14 days after being injected with MFNP-labeled mMSCs. Its left wound had been exposed to the magnetic field (highlighted by arrows). c) Photos showing gradual closure of the wounds over time after mice were treated with MFNP-labeled mMSCs. Upper and lower rows of photos showed the left side (with magnet) and right side (without magnet) wounds, respectively, of a representative mouse. d) The closure of wound areas over time. The wound sizes were measured by a caliper and calculated as the area at 1 day, 3 day, 7 day, and 14 day. Error bars were based standard deviations (SD) of eight mice per group. e,f) H&E stained images of wound slices with (e) and without (f) magnetically induced stem cell accumulation 2 weeks after injection of MFNP-labeled mMSCs. P-values: ∗, $p < 0.01$. Abbreviations: Ep, epidermis; F, hair follicle; M, muscle.

a new type of multifunctional probes to track and control the translocation of stem cells in vivo, and encourage further exploration of imaging-guided remotely-controlled cell therapies for better specificity and enhanced efficacy.

4. Experimental Section

Materials: All chemicals involved in this work were analytical grade and used without further purification. Y_2O_3, Yb_2O_3 and Er_2O_3 were purchased from Shanghai Chemical Industrial Co. All the rare-earth trifluoroacetates were prepared by dissolving the respective rare-earth oxides in trifluoroacetic acid (CF_3COOH, Shanghai Chemical Industrial Co.). Oleic acid (OA, 90%), oleyl amine (OM) and 1-octadecene (ODE >90%) were purchased from Sigma-Aldrich. Benzyl ether, 1, 2-dexadecanediol (97%), diethylene glycol, iron acetylacetonate (Fe $(acac)_3$), (α+) lipoic acid (LA), and dopamine (DA) were also purchased from Sigma-Aldrich.

Synthesis of MFNPs: MFNPs were synthesized following our previously reported procedure.[31] Based on a well-established protocol,[27,59–61] we firstly synthesized $NaYF_4$: Yb, Er (Y:Yb:Er = 69:30:1) nanoparticles with their surface modified by poly(acrylic acid) (PAA). Ultrasmall Fe_3O_4 nanoparticles (IONPs) were also synthesized and surface-modified by dopamine (DA). Secondly, DA modified IONPs in water were slowly added into PAA modified UCNPs under ultrasonication for 1 h. After stirring for 5 h, excess IONPs were removed by centrifugation at 6000 rpm, obtaining a UCNP-IONP composite. After gold seeds were attached on the surface of UCNP-IONP, an aged Au growth solution was then added, offering a thin gold shell grown on the surface of UCNO-IONP composite. The obtained MFNPs were then functionalized with LA-PEG to acquire water solubility and stability in physiological solutions.

Characterization: Scanning electron microscopy (SEM) images were taken by using a FEI Quanta 200F scanning electron microscope. Transmission electron microscopy (TEM) and high-resolution TEM (HR-TEM) images were obtained using a FEI Tecnai F20 transmission electron microscope at an acceleration voltage of 200 kV. Upconversion fluorescence spectra were obtained on a FluoroMax 4 luminescence spectrometer (HORIBA Jobin Yvon) with an external 980 nm laser diode (1 W, continuous wave with 1 m fiber, Beijing Hi-Tech Optoelectronics CO., Ltd) as the excitation source. UV-vis-NIR spectra were recorded by a PerkinElmer Lambda 750 UV-vis-NIR spectrophotometer.

Isolation and Expansion of mMSCs: mMSCs were obtained from BALB/c mice. Mice of 8 to 10 weeks old were individually killed by CO_2. The femurs and tibiae were collected, and ends of each tibia and femur were clipped to expose the bone marrow. Then the marrow was flushed by low glucose-Dulbecco's modified Eagle medium(L-DMED) medium constituted of 10% fetal calf serum, glutamine 4 mM and 1% penicillin/streptomycin. Cells were then washed twice in a medium and plated in a Petri dish at a density of 2×10^6 cells/cm^2. After 3 days, non-adherent cells were removed by washing with PBS two to three times. Adherent cells were trypsinized, replanted for expansion and grown to 80% confluence with medium changed every 3–4 days. All cell cultures were maintained under the 5% CO_2 atmosphere at 37 °C.

Cell Labeling with MFNPs: MFNP-PEG at various concentrations were incubated with mMSCs in 24-well culture plates for 4 h, followed by repeated washing with PBS to remove unlabeled MFNP-PEG. Confocal luminescence imaging of cells was performed with a modified Leica laser-scanning microscope using a 980 nm external laser as the excitation source.

mMSCs Transfected with Green Fluorescent Protein (GFP): mMSC were transduced with a lenti-virus (pFU vector) carrying a fusion GFP reporter gene. The GFP expressing Lentiviral vector was a gift from

Prof. Yun Zhao at Soochow University. Transductions were performed in 3 cm diameter 6-well plates ($5 \times 10^4 - 1 \times 10^5$ cells/well). After 24 h, transfected cells were washed twice with PBS and cultured in L-DMEM medium until analysis and use.

LDH Assay: The cell membrane integrity can be determined by lactate dehydrogenase (LDH) leakage assay. LDH leakage was measured using a cytotoxicity detection kit (Promega Cat. 7891) following the vendor's protocol. In this experiment, mMSCs lysed by 1% Triton-X-100 were used as the positive control, while the cell-free medium was used as the negative control. The analysis was performed using a microplate reader (Bio-Rad).

ROS Assay: ROS production was evaluated by a hydroethidine (DHE) probe known be oxidized by various oxidative agents. In brief, cells were treated with different concentrations of MFNP-PEG for 1 day. After trypsination, cells were centrifuged at 1000 min/r for 5 min, re-suspended in cell culture medium containing 1 μM HE (sigma), and analyzed using a flow cytometry (FACS Calibur from Becton, Dickinson and Company).

Differentiation of MFNP-Labeled mMSCs: Differentiation capacity of mMSCs was assessed by adipogenic and osteogenic differentiation-induction experiments. For adipogenic differentiation, mMSCs with or without MFNP-PEG labeling were plated at a density of 2×10^4 cells/cm^2 in a 24-well culture plate. When the cells reached confluent, adipogenic differentiation was initiated by adding an induction culture containing L-DMEM cell medium supplemented with 10% FBS, 1 μM dexamethasone, 60 μM indomethacin, 5 μg/mL insulin, and 0.5 mM 3-isobutyl-l-methylxanthine. The induction medium was changed every 3 days in 2 weeks. Cells were then fixed and stained with 0.3% Oil-red-O.

The osteogenic induction culture was L-DMEM supplemented with 10% FBS, 0.1 μM dexamethasone, 50 mg/L ascorbic acid, and 10 mM β-glycerophosphate. The culture medium was replaced every 3-4 days. After being cultured for 2 weeks, cells were fixed and stained by Alizarin red S.

In Vivo Multimodal Imaging: MFNP-labeled mMSCs (10, 10^2, 10^3, and 10^4 cells) suspended in PBS were subcutaneously transplanted into the back of athymic nude mice. A modified Maestro in vivo imaging system using a 980 nm optical fiber-coupled laser as the excitation source was employed to image the mice. The laser power density was ≈0.4 W/cm^2 during imaging (exposure time = 20 s). An 850 nm short-pass emission filter was applied to prevent the interference of excitation light to the CCD camera.

MR imaging studies were conducted on a 3-T clinical MRI scanner (Bruker Biospin Corporation, Billerica, MA, USA) equipped with a special coil designed for small animal imaging.

Magnetically Induced Tissue Repairing by Stem Cells: BALB/c mice (8 weeks old; female; body weight, 20–23 g) were obtained from Suzhou Belda Bio-Pharmaceutical Co. and performed under protocols approved by Soochow University Laboratory Animal Center. For magnetic wound targeting, the same two wounds (d ≈ 0.8 cm) were drawn at the abdomen of each mouse following a literature protocol.[58] In brief, after hair removal from the dorsal surface and anesthesia, two 8-mm full-thickness excisional skin wounds were created on each side of the midline. The tegaderm was placed over the wounds to stabilize the wound position. The animals were housed individually. After one day, MFNP-labeled mMSCs were i.p. injected into the center of the abdomen of each mouse. Magnetic targeting was conducted by attaching a small magnet onto one side of the wounds for 6 h right after injection of cells. A totally of 8 mice were used in this study. The wound sizes were measured by a caliper and calculated as the area at 1 day, 3 day, 7 day, and 14 day. For statistic comparison, P values were calculated by the student's t-test.

Supporting Information

Supporting Information is available from the Wiley Online Library or from the author.

Acknowledgements

L.C. and C.W. contributed equally to this work. This work was partially supported by the National Basic Research Programs of China (973 Program) (2012CB932601, 2011CB911002), the National Natural Science Foundation of China (51132006, 51002100), and a Project Funded by the Priority Academic Program Development of Jiangsu Higher Education Institutions. L.C. was supported by the Innovation Program of Graduate Students in Jiangsu Province (CX10B_036Z).

Received: June 26, 2012
Revised: August 2, 2012
Published online: August 22, 2012

[1] C. Ren, S. Kumar, D. Chanda, L. Kallman, J. Chen, J. D. Mountz, S. Ponnazhagan, *Gene Ther.* **2008**, *15*, 1446.
[2] C. P. Hodgkinson, J. A. Gomez, M. Mirotsou, V. J. Dzau, *Hum. Gene Ther.* **2010**, *21*, 1513.
[3] F.M. Chen, L.A. Wu, M. Zhang, R. Zhang, H. H. Sun, *Biomaterials* **2011**, *32*, 3189.
[4] C. Ren, S. Kumar, D. Chanda, J. Chen, J. D. Mountz, S. Ponnazhagan, *Stem Cells* **2008**, *26*, 2332.
[5] B. Hall, J. Dembinski, A. K. Sasser, M. Studeny, M. Andreeff, F. Marini, *Int. J. Hematol.* **2007**, *86*, 8.
[6] K. S. Aboody, J. Najbauer, M. K. Danks, *Gene Ther.* **2008**, *15*, 739.
[7] H. Wang, F. Cao, A. De, Y. Cao, C. Contag, S. S. Gambhir, J. C. Wu, X. Chen, *Stem Cells* **2009**, *27*, 1548.
[8] I. M. Barbash, P. Chouraqui, J. Baron, M. S. Feinberg, S. Etzion, A. Tessone, L. Miller, E. Guetta, D. Zipori, L. H. Kedes, R. A. Kloner, J. Leor, *Circulation* **2003**, *108*, 863.
[9] L. Ferreira, J. M. Karp, L. Nobre, R. Langer, *Cell Stem Cell* **2008**, *3*, 136.
[10] A. B. Rosen, D. J. Kelly, A. J. T. Schuldt, J. Lu, I. A. Potapova, S. V. Doronin, K. J. Robichaud, R. B. Robinson, M. R. Rosen, P. R. Brink, G. R. Gaudette, I. S. Cohen, *Stem Cells* **2007**, *25*, 2128.
[11] B. S. Shah, P. A. Clark, E. K. Moioli, M. A. Stroscio, J. J. Mao, *Nano Lett.* **2007**, *7*, 3071.
[12] S. Lin, X. Xie, M. R. Patel, Y.-H. Yang, Z. Li, F. Cao, O. Gheysens, Y. Zhang, S. S. Gambhir, J. H. Rao, J. C. Wu, *BMC Biotechnol.* **2007**, *67*, 1472.
[13] T. H. Chung, J. K. Hsiao, S. C. Hsu, M. Yao, Y. C. Chen, S. W. Wang, M. Y. P. Kuo, C. S. Yang, D. M. Huang, *ACS Nano* **2011**, *12*, 9807.
[14] H. Kim, H. M. Dae, C. Park, E. O. Kim, D. Kim, I. H. Kim, Y. H. Kim, Y. Choi, *J. Mater. Chem.* **2011**, *21*, 7742.
[15] T. Kim, E. Momin, J. Choi, K. Yuan, H. Zaidi, J. Kim, M. Park, N. Lee, M. T. McMahon, A. Quinones-Hinojos, J. W. M. Bulte, T. Hyeon, A. A. Gilad, *J. Am. Chem. Soc* **2011**, *133*, 2955.
[16] C. Wang, X. Ma, S. Ye, L. Cheng, K. Yang, L. Guo, C. Li, Y. Li, Z. Liu, *Adv. Funct. Mater.* **2012**, *22*, 2363.
[17] C. W. Lu, Y. Hung, J. K. Hsiao, M. Yao, T. H. Chung, Y. S. Lin, S. H. Wu, S. C. Hsu, H. M. Liu, C. Y. Mou, C. S. Yang, D. M. Huang, Y. C. Chen, *Nano Lett.* **2007**, *7*, 149.
[18] H. Yukawa, Y. Kagami, M. Watanabe, K. Oishi, Y. Miyamoto, Y. Okamoto, M. Tokeshi, N. Kaji, H. Noguchi, K. Ono, M. Sawada, Y. Bab, N. Hamajima, S. Hayashi, *Biomaterials* **2010**, *31*, 4094.
[19] A. Aicher, W. Brenner, M. Zuhayra, C. Badorff, S. Massoudi, B. Assmus, T. Eckey, E. Henze, A. M. Zeiher, S. Dimmeler, *Circulation* **2003**, *107*, 2134.
[20] F. Wang, R. Deng, J. Wang, Q. Wang, Y. Han, H. Zhu, X. Chen, X. Liu, *Nat. Mater.* **2011**, *10*, 968.
[21] J. Zhou, Z. Liu, F. Li, *Chem. Soc. Rev.* **2012**, *41*, 1323.
[22] G. Tian, Z. Gu, L. Zhou, W. Yin, X. Liu, L. Yan, S. Jin, W. Ren, G. Xing, S. Li, Y. Zhao, *Adv. Mater.* **2012**, *24*, 1226.

[23] J. Liu, Y. Liu, Q. Liu, C. Li, L. Sun, F. Li, *J. Am. Chem. Soc.* **2011**, *133*, 15276.
[24] M. Nyk, R. Kumar, T. Y. Ohulchanskyy, E. J. Bergey, P. N. Prasad, *Nano Lett.* **2008**, *8*, 3834.
[25] L. Wang, R. Yan, Z. Huo, L. Wang, J. Zeng, J. Bao, X. Wang, Q. Peng, Y. Li, *Angew. Chem. Int. Ed.* **2005**, *44*, 6054.
[26] H. S. Qian, H. C. Guo, P. C. L. Ho, R. Mahendran, Y. Zhang, *Small* **2009**, *5*, 2285.
[27] L. Xiong, T. Yang, Y. Yang, C. Xu, F. Li, *Biomaterials* **2010**, *31*, 7078.
[28] L. Cheng, K. Yang, X. Lu, M. Shao, Z. Liu, *Nanomedicine* **2011**, *6*, 1327.
[29] R. A. Jalil, Y. Zhang, *Biomaterials* **2008**, *29*, 4122.
[30] L. Xiong, Z. Chen, Q. Tian, T. Cao, C. Xu, F. Li, *Anal. Chem.* **2009**, *81*, 8687.
[31] L. Cheng, K. Yang, Y. Li, J. Chen, C. Wang, M. Shao, S.-T. Lee, Z. Liu, *Angew. Chem. Int. Ed* **2011**, *50*, 7385.
[32] L. Cheng, K. Yang, Y. Li, X. Zeng, M. Shao, S. T. Lee, Z. Liu, *Biomaterials* **2012**, *33*, 2215.
[33] C. Wang, L. Cheng, Z. Liu, *Biomaterials* **2011**, *32*, 1110.
[34] F. Chen, W. Bu, S. Zhang, X. Liu, J. Liu, H. Xing, Q. Xiao, L. Zhou, W. Peng, L. Wang, J. Shi, *Adv. Funct. Mater* **2011**, *21*, 4285.
[35] H. Xing, W. Bu, S. Zhang, X. Zheng, M. Li, F. Chen, Q. He, L. Zhou, W. Peng, Y. Hua, J. Shi, *Biomaterials* **2012**, *33*, 1079.
[36] L. Cheng, K. Yang, S. Zhang, M. Shao, S. Lee, *Nano Res.* **2010**, *3*, 722.
[37] J. Zhou, M. Yu, Y. Sun, X. Zhang, X. Zhu, Z. Wu, D. Wu, F. Li, *Biomaterials* **2011**, *32*, 1148.
[38] Q. Liu, Y. Sun, T. Yang, W. Feng, C. Li, F. Li, *J. Am. Chem. Soc.* **2011**, *133*, 17122.
[39] C. Wang, L. Cheng, H. Xu, Z. Liu, *Biomaterials* **2012**, *33*, 4872.
[40] Y. Chen, H. Chen, D. Zeng, Y. Tian, F. Chen, J. Feng, J. Shi, *ACS Nano* **2010**, *4*, 6001.
[41] S. Xu, A. D. Becker, B. V. Camp, K. Vanderkerken, I. V. Riet, *J. Biomed. Biotechnol.* **2010**, *10*, 105940.
[42] P. Bianco, P. G. Robey, P. J. Simmons, *Cell Stem Cell* **2008**, *2*, 313.
[43] S. C. Silverstein, R. M. Steinman, Z. A. Cohn, *Annu. Rev. Biochem.* **1977**, *46*, 669.
[44] J. V. Frangioni, R. J. Hajjar, *Circulation* **2004**, *110*, 3378.
[45] K. Hoshino, H. Q. Ly, J. V. Frangioni, R. J. Hajjar, *Prog. Cardiovasc. Dis.* **2007**, *49*, 414.
[46] D. J. P. Donald G. Phinney, *Stem Cells* **2007**, *25*, 2896.
[47] D. J. Prockop, C. A. Gregory, J. L. Spees, *Proc. Natl. Acad. Sci. USA* **2003**, *100*, 11917.
[48] D. L. Kraitchman, M. Tatsumi, W. D. Gilson, T. Ishimori, D. Kedziorek, P. Walczak, P. Segars, H. H. Chen, D. Fritzges, I. Izbudak, R. G. Young, M. Marcelino, M. F. Pittenger, M. Solaiyappan, R. C. Boston, B. M. W. Tsui, R. L. Wahl, J. W. M. Bulte, *Circulation* **2005**, *112*, 1451.
[49] J. Wang, F. Wang, C. Wang, Z. Liu, X. Liu, *Angew. Chem. Int. Ed.* **2011**, *50*, 10369.
[50] T. Yang, Y. Sun, Q. Liu, W. Feng, P. Yang, F. Li, *Biomaterials* **2012**, *33*, 3733.
[51] E. S. Jang, J. H. Shin, G. Ren, M.-J. Park, K. Cheng, X. Chen, J. C. Wu, J. B. Sunwoo, Z. Cheng, *Biomaterials* **2012**, *33*, 5584.
[52] J. Riegler, J. A. Wells, P. G. Kyrtatos, A. N. Price, Q. A. Pankhust, M. F. Lythgoe, *Biomaterials* **2010**, *31*, 5366.
[53] B. Polyak, I. Fishbein, M. Chorny, I. Alferiev, D. Williams, B. Yellen, G. Friedman, R. J. Levy, *Proc. Natl. Acad. Sci. USA* **2008**, *105*, 698.
[54] B. Panagiotis G. Kyrtatos, P. Lehtolainen, M. Junemann-Ramirez, A. Garcia-Prieto, A. N. Price, J. F. Martin, D. David G. Gadian, Q. A. Pankhurst, M. F. Lythgoe, *J Am. Coll. Cardiol. Intv.* **2009**, *2*, 794.
[55] S. V. Pislaru, A. Harbuzariu, R. Gulati, T. Witt, N. P. Sandhu, R. D. Simari, G. S. Sandhu, *J Am. Coll. Cardiol. Intv.* **2006**, *48*, 1839.
[56] P. Bianco, P. G. Robey, *Nature* **2001**, *414*, 118.
[57] R. D. Gallano, V. Joseph Michaels, M. Dobryansky, J. P. Levine, G. C. Gurtner, *Wound Rep. Reg.* **2004**, *12*, 485.
[58] Y. Wu, L. Chen, P. G. Scott, E. E. Tresget, *Stem Cells* **2007**, *25*, 2648.
[59] G. S. Yi, G. M. Chow, *Adv. Funct. Mater.* **2006**, *16*, 2324.
[60] H. Mai, Y. Zhang, R. Si, Z. Yan, L. Sun, L. You, C. Yan, *J. Am. Chem. Soc.* **2006**, *128*, 6426.
[61] S. Sun, H. Zeng, D. B. Robinson, S. Raoux, P. M. Rice, S. X. Wang, G. Li, *J. Am. Chem. Soc.* **2004**, *126*, 273.